JOURNAL OF SOLID STATE CHEMISTRY 48, 357–367 (1983)

The Preparation and Selected Properties of Mg-Doped *p*-Type Iron Oxide as a Photocathode for the Photoelectrolysis of Water Using Visible Light

C. LEYGRAF, M. HENDEWERK, AND G. SOMORJAI

Materials and Molecular Research Division, Lawrence Berkeley Laboratory and Department of Chemistry, University of California, Berkeley, California 94720

Received December 20, 1982; in revised form March 7, 1983

Stable Mg-doped iron oxides that exhibit *p*-type character have been synthesized. These have been utilized in the form of sintered polycrystalline disks for the photodissociation of water. We report the influence of sintering temperature, surface oxygen deficiency, Mg-doping level, and solution chemistry on the photoactivity of the Mg-doped iron oxide photocathodes.

Introduction

α-Fe_2O_3 is one of the widely investigated semiconductors for the photoinduced dissociation of water. This compound has a relatively small band gap, 2.2 eV (*1*), that permits the use of about 40% of the solar photon flux incident on the earth's surface. It is abundant and therefore inexpensive and it is stable in various aqueous solutions over a broad pH range. However, when using pure α-Fe_2O_3, an external potential is needed, in addition to illumination, to produce hydrogen and oxygen from water. Various ways to eliminate the need to use an external potential have been explored (*2–5*). Recently, we reported that a *p/n* iron oxide diode assembly composed of magnesium- and silicon-doped polycrystalline disks produces hydrogen from water with visible light and without any external potential (*6*).

One would expect that introducing Ca^{2+} or Mg^{2+} ions into the α-Fe_2O_3 lattice to substitute for Fe^{3+} ions would increase the concentration of electron vacancies in this electronic semiconductor and would result in *p*-type behavior. In other laboratories, both CaO and MgO have been used to dope α-Fe_2O_3 but no *p*-type photocurrents were observed (*7*). Other workers have found *p*-type behavior of iron oxides but no photoelectrochemical measurements were made (*8, 9*). We succeeded in preparing *p*-type α-Fe_2O_3 by doping with MgO and changing the conditions for its preparation. We then studied the photodissociation of water by these *p*-type iron oxide polycrystalline disks in a *p/n* diode assembly (*6*). In this paper the preparation of the MgO-doped α-Fe_2O_3 is described and evidence is presented which shows that the photoactivity of the *p*-type iron oxide is markedly influenced by various experimental parame-

0022-4596/83 $3.00

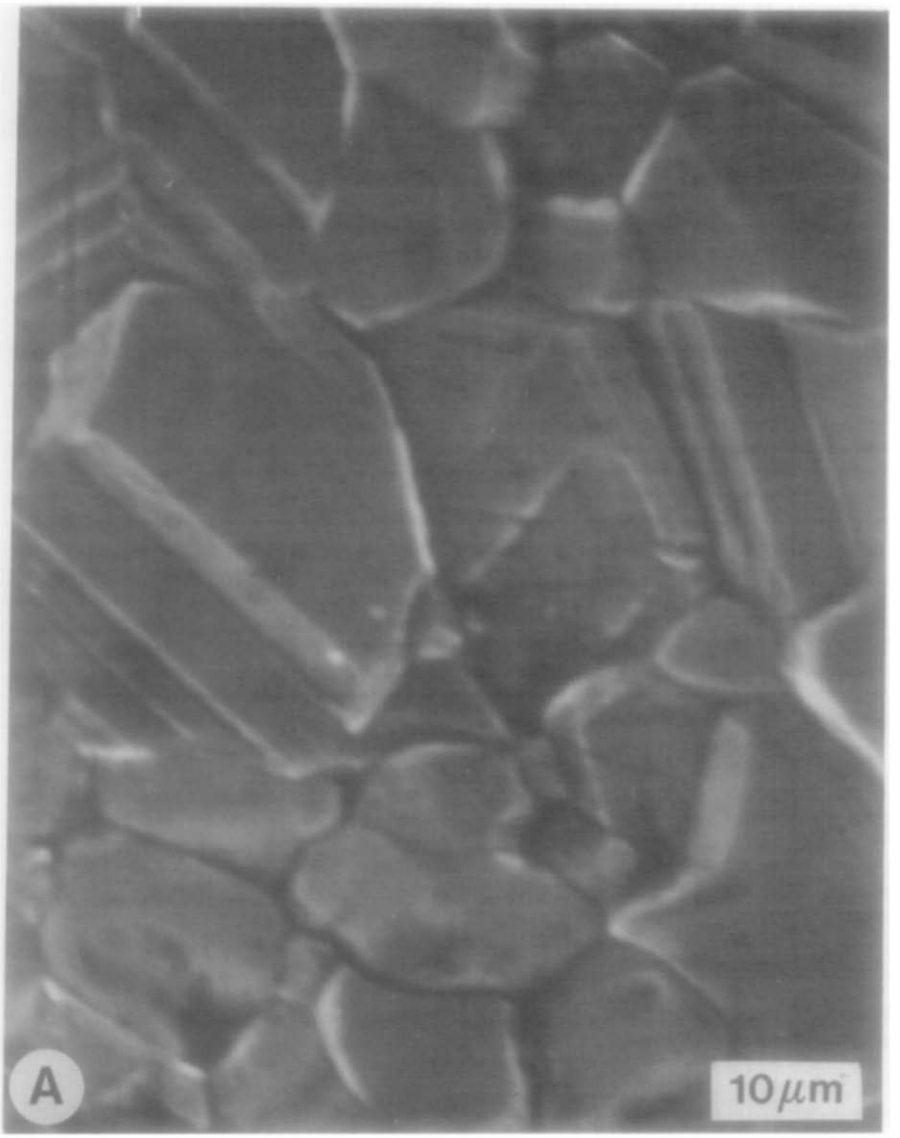

FIG. 1. Scanning electron microscopy photographs of sintered and water quenched *p*-type iron oxide with Mg/(Mg + Fe) = 5 at.%. Sintering temperatures 1350°C (A) and 1480°C (B).

ters. These include sintering temperature, iron oxide surface conditions, and electrolyte composition.

Synthesis and Characterization of MgO-doped p-type α-Fe_2O_3

Samples were prepared by mixing powders of α-Fe_2O_3 (MCB Manufacturing Chemists, reagent grade) and MgO (Mallinckrodt, analytical reagent grade). Four concentration levels of MgO were used such that the atomic percent of magnesium (Mg/(Mg + Fe)) was 1, 5, 10, or 20. The mixed powders were pressed (7000 Kg/cm^2) to form pellets 10 mm in diameter and subsequently sintered in air at 1350, 1425, or

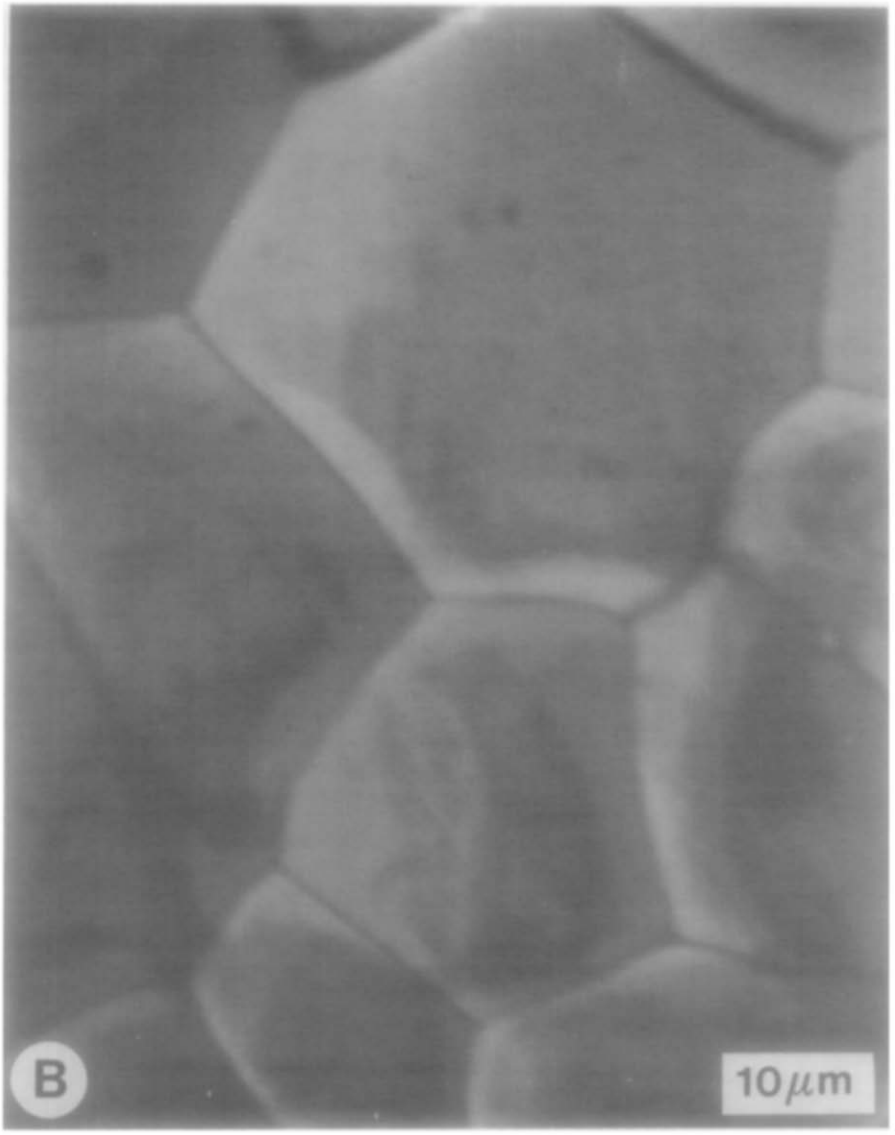

FIG. 1—*Continued.*

1480°C for 20 hr. The disks were then rapidly cooled in water to room temperature when removed from the oven and had dark resistivities ranging from 10^1 to 10^3 Ω cm (Table I).

Sample characterization by means of X-ray diffraction, scanning electron microscopy, and scanning auger electron microscopy all showed that the magnesium iron oxides consist mainly of a Mg-doped Fe_2O_3 matrix (Table I). At 1350°C all peaks in the X-ray spectrum corresponded to an α-Fe_2O_3 phase, whereas at 1480°C several of the α-Fe_2O_3 peaks were missing and peaks appeared which indicated the presence of $MgFe_2O_4$ and other substances which could not be identified.

Scanning electron microscopy pictures shown in Fig. 1 depict the changes in surface topography with varied sintering tem-

TABLE I

SAMPLE CHARACTERIZATION OF *p*-TYPE Mg-DOPED IRON OXIDES

Sample	Mg/Mg + Fe atom	Sintering temperature (°C)	Resistivity (Ω cm)
Mg/(Mg + Fe) = 1 atom	≤1	1350	10^6–
5		1350	10^3–10^4
10	6–8	1350	10^3–10^4
20		1350	10 –10^2
5		1350	10^3–10^4
5		1425	10^2–10^3
5		1480	10 –10^2

perature. At 1350°C the grains range in size from 10 to 20 μm in diameter and appear to be somewhat faceted, while at 1480°C the grains are larger, 20 to 50 μm with much smoother surfaces. X-ray photoelectron spectroscopy (ESCA) measurements of the O(1*s*) peaks in the Mg-doped iron oxides are shown in Fig. 2. The lower binding energy peak is due to the lattice oxygen ions O^{2-} (529.2 eV) and the higher binding energy peak corresponds to both adsorbed oxygen and hydroxyl groups (532.0 eV) (*10*).

The photoelectrochemical experiments were conducted in a standard three electrode electrochemical cell with a Mercuric Oxide Luggin Capillary reference electrode, a *p*-type iron oxide disk connected to a metal wire with silver epoxy as the cathode, and a Pt counter electrode. Silicon rubber sealant was used to isolate the metal wire (Pt or Khantal) and silver epoxy from the solution. Inlet and outlet valves were attached to permit oxygen gas to be purged through the solution below the level of the liquid, pass over the sample, and be forced out of the cell from above the solution.

Illumination of the sample was accomplished using a 500-W Tungsten halogen lamp. The light was focused with quartz optics and filtered first through a 5-cm water cell to absorb most of the ir radiation to

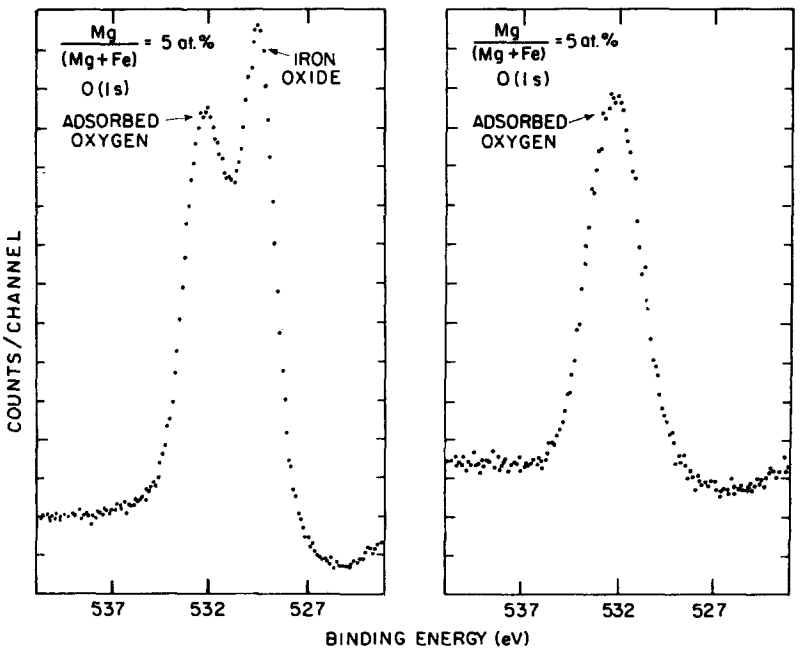

FIG. 2. X-ray photoelectron spectra of Mg-doped iron oxide before (left) and after (right) oxygen purging.

avoid heating effects, then through a Corning 3-72 visible pass filter to screen the uv radiation with photons of $h\nu \geq 2.7$ eV. After measuring the irradiance with a thermopile detector and taking into account the absorption of light by the electrolyte solution and the filters, the incoming power of visible light was 37 ± 1 mW. All results presented in this work were accumulated under potentiostatic steady state conditions with the use of a Pine RDE 3 potentiostat. Voltage readings are presented vs the reversible hydrogen electrode (RHE), the hydrogen electrode at the pH of the solution.

The electrolyte solutions used in the electrochemical cell were sodium hydroxide and sodium sulfate. The sodium hydroxide solutions were made by diluting a 10 *N* concentrated NaOH solution (Fisher Scientific Co.) with distilled water. Anhydrous sodium sulfate powder (Baker) with a nominal purity of 99.9% was used to prepare the 0.1 *M* Na_2SO_4 solutions.

Results

The photocurrents obtained with illumination of the Mg-doped iron oxide disks used as cathodes in a *p/n* diode assembly are directly proportional to the amount of hydrogen that can be produced by the photodissociation of water (*6*). The results of preparative methods are presented followed by the photoactivity differences that were obtained by varying the dopant levels of magnesium, altering sintering temperature, changing the pH of the electrolytic solution, and subjecting the samples to oxidative conditions. Our results are presented in terms of the photocurrents defined as the difference in magnitude of the current obtained under illumination and in the dark. The data are plotted in the figures as current densities ($\mu A/cm^2$) against the applied potential voltage with respect to a reversible hydrogen electrode RHE. The dark currents are not displayed, but they are smaller and within the same order of magnitude as the photocurrents.

3.1 Influence of Sintering Temperature on the Photoconductivity of the Mg-Doped Iron Oxide.

In a photovoltaic cell, a low resistivity of the working electrode is of crucial importance. High resistivities may be the reason why earlier studies on Mg-doped iron oxide gave no measurable photocurrents (*7*). By sintering samples of iron oxide with Mg/(Mg + Fe) = 5 at.% at temperatures of 1425–1480°C and rapidly quenching them in water, dark resistivities in the range of 10^1–10^2 Ω cm were obtained. When cooling from the sintering temperature was in air and at a much slower rate, much higher sample resistivities of the order of 10^3–10^5 Ω cm were obtained (see Table I). The same table also shows that sintering the pellets at temperatures of 1350°C or lower resulted in higher resistivities and that the resistivity at a given sintering temperature increased with decreasing doping level. Photocurrents of 5% Mg-doped samples sintered at three temperatures are shown in Fig. 3. A marked influence of sintering temperatures on photocurrent is observed with the photoactivity increasing in the order of 1480 < 1350 < 1425°C.

3.2 The Effect of Oxygen Purging of the Electrolyte Solution on the Photocurrent

It was observed that purging the electrolyte with oxygen gas increases the photocurrents (and dark currents) of the *p*-type iron oxide samples. The effect of oxygen purging for 5 min is seen in Fig. 4 for the same Mg-doped iron oxide disks as shown in Fig. 3. Before oxygen purging there is a wide variation in the photocurrents of samples sintered at the three different temperatures of 1350, 1425, and 1480°C. After oxygen purging the photocurrents are higher in magnitude and the photoactivity of all three samples appears to be very similar. Al-

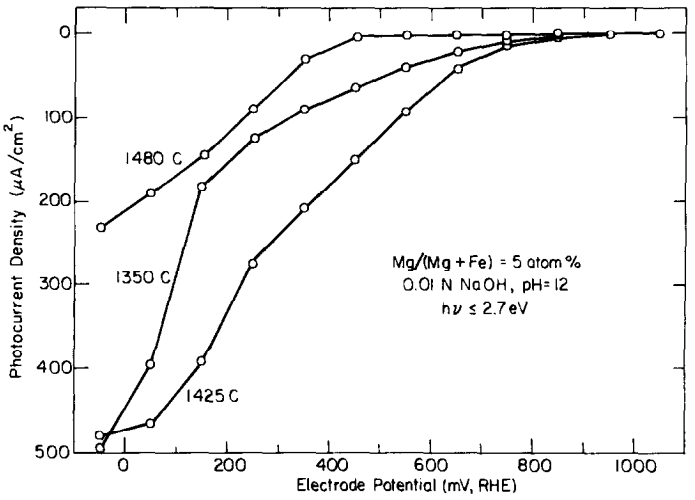

FIG. 3. Photocurrent density as a function of electrode potential in 0.01 *N* NaOH for various sintering temperatures. Mg/(Mg + Fe) = 5 at.%.

though the photocurrent of the 1350°C sintered sample after oxygen purging is slightly lower than the photocurrents of the samples sintered at 1425 and 1480°C, it should be noted that the resistivities of the 1425 and 1480°C sintered samples were the

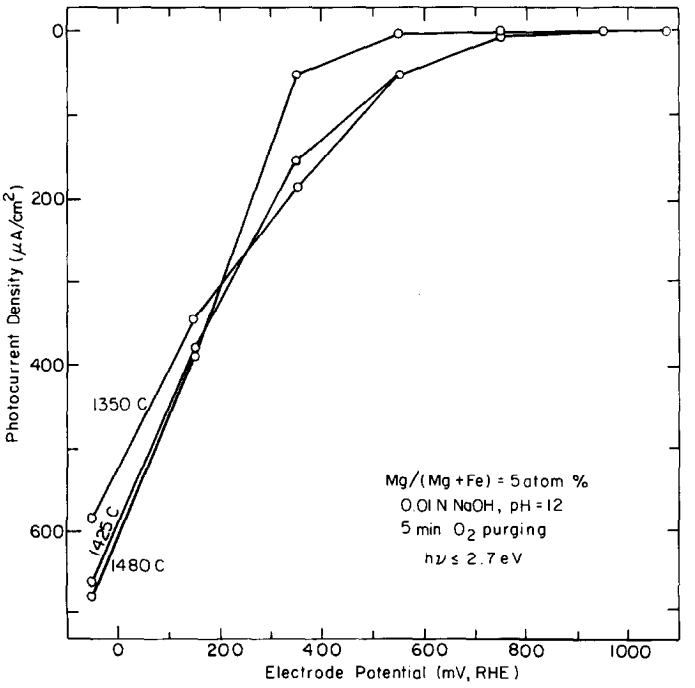

FIG. 4. Photocurrent density as a function of electrode potential for various sintering temperatures and after oxygen purging the 0.01 *N* NaOH solution for 5 min. Mg/(Mg + Fe) = 5 at.%.

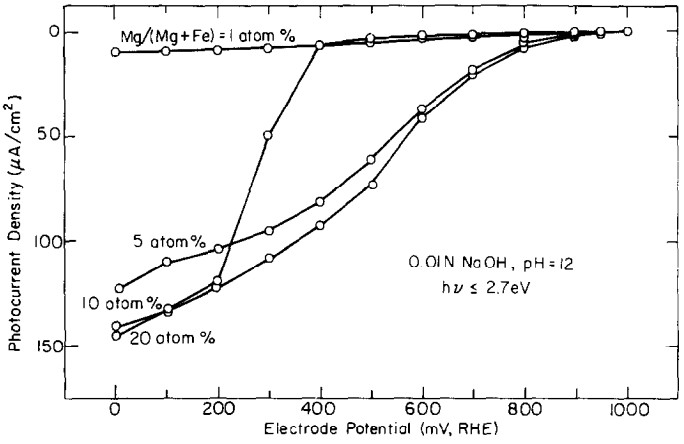

FIG. 5. Photocurrent density as a function of electrode potential for various Mg-doped iron oxides in 0.01 *N* NaOH.

same (50 Ω cm) within the experimental accuracy, while that of the 1350°C sintered sample was higher (5000 Ω cm).

3.3 Photocurrent Response to Variations in Mg Dopant Levels

Four oxides were prepared and studied under identical conditions except that the atomic percent of magnesium (Mg/(Mg + Fe)) was altered between 1, 5, 10, and 20%. All samples were sintered at 1425°C. Photocurrents measured in an 0.01 *N* NaOH electrolyte solution are shown in Fig. 5. The samples doped with 5 and 10% Mg have an onset potential of 950 ± 50 mV vs RHE and exhibit photocurrents which increase monotomically with a more cathodic applied potential. The 20% doped oxide has an onset potential approximately 125 mV more negative than for samples with 5 and

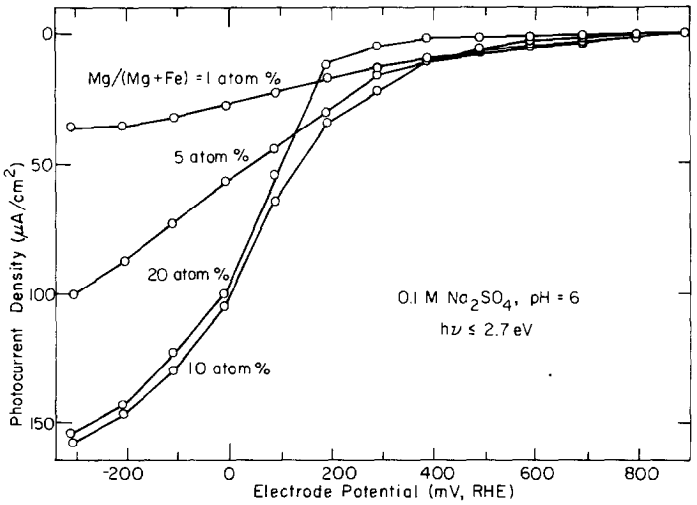

FIG. 6. Photocurrent density as a function of electrode potential for various Mg-doped iron oxides in 0.1 *M* Na_2SO_4.

10% doping levels but the photocurrent rises steeply so that 5, 10, and 20% doping levels differ only slightly once very cathodic potentials are reached (100–200 mV vs RHE). The photocurrents when only 1% magnesium doping was used were quite low. A corresponding study carried out in a 0.1 *M* Na_2SO_4 solution (Fig. 6) yielded qualitatively identical results although the magnitudes of the current densities are somewhat higher.

3.4 pH Dependence of the Photocurrents

Figure 7 depicts the results of measurements taken from a single *p*-type iron oxide sample in electrolytic solutions of 1, 10^{-2}, and 10^{-4} *N* NaOH. The largest photocurrents were obtained in the 10^{-2} *N* solution with slightly lower values in the 1 *N* solution. The photoactivity in 10^{-4} *N* NaOH was low and relatively constant even when extensively polarized.

3.5 Stability of the Photocurrents of the Mg-Doped Iron Oxide Samples

During prolonged polarization of the order of 10 hr, the photocurrents of Mg-doped samples showed no measurable alteration. Visual inspection of the iron oxide cathodes after the electrochemical measurements in the aqueous solutions of different pH in the range of 6 to 14 showed no signs of corrosion. In fact, the photocurrents of a 5 at.% Mg-doped sample polarized at 600 mV (RHE) in the 0.01 *N* NaOH solution increased over an 8-hr period by 50% and in the 0.1 *M* Na_2SO_4 solution by 30% during the same time span (*6*). Other workers have also found Fe_2O_3 to be extremely stable even under anodic polarization (*11–13*).

Discussion

DC conductivity and Seebeck voltage measurements of pure α-Fe_2O_3 have shown that above 1000°C the ferric oxide equilibrates with the surrounding oxygen containing atmosphere (*9*). From the increase in oxygen deficiency with increasing temperature (*14*) a corresponding increase in conductivity has been observed (*9*). These earlier findings are in qualitative agreement with our study which shows an increase in conductivity with sintering temperature (Table I). The importance of rapid quenching from the sintering temperature to obtain high conductivity samples can be explained by the tendency of ferric oxides to adsorb oxygen at grain boundaries below 450°C re-

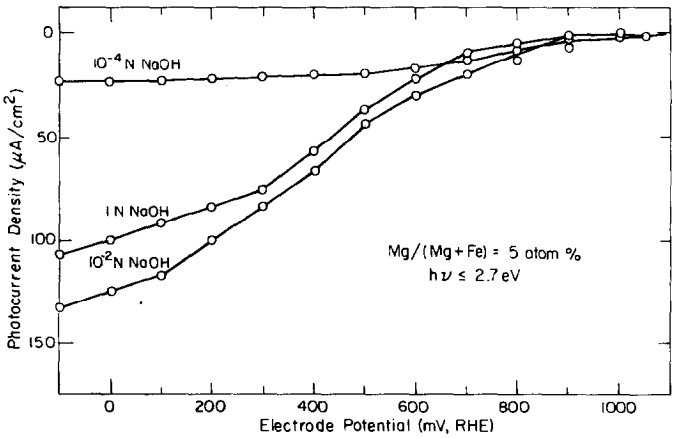

FIG. 7. Photocurrent density as a function of electrode potential for various concentrations of NaOH solutions. Mg/(Mg + Fe) = 5 at.%.

sulting in a decrease in conductivity (*15*). This was illustrated in our study by exposing samples containing 5 at.% Mg and which had been rapidly quenched from 1480°C to a subsequent anneal for 2 hr in flowing oxygen at 500 and 800°C, respectively. Slow cooling from these temperatures resulted in resistivities of around 5×10^4 and $>10^6$ Ω cm, respectively, as opposed to 50 Ω cm after rapid quenching from 1480°C.

Because of its high oxygen vacancy concentration obtained at higher (>1000°C) temperatures ferric oxide has been classified as an *n*-type oxide semiconductor (*9*). The undoped ferric oxide shows solely *n*-type behavior in photoelectrochemical measurements despite being produced by a great variety of sample preparation techniques (*11–13, 16*). When introducing magnesium into the ferric oxide lattice, each Mg^{2+} ion contributes one positive carrier (*17*). The Mg-doped iron oxide samples exhibit *p*-type behavior in the whole investigated Mg-concentration region of 1–20 at.%. We find that the conductivities of the Mg-doped samples increase with Mg-dopant concentration (Table I).

Sintering at different temperatures results in photocurrents which are higher in samples sintered at 1350 and 1425°C than at 1480°C (Fig. 3). The oxygen deficiency at elevated temperatures may result in the formation of a surface region containing Fe_3O_4 or Mg-doped Fe_3O_4 (undetectable by X-ray analysis), with amounts that increase with sintering temperature. It has been suggested (*18*) that the presence of Fe_3O_4 in the surface layer decreases the photoactivity because of recombination of holes and mobile electrons in the highly conductive surface region. The presence of an oxygen deficient, Fe_3O_4-containing surface layer could then also explain the loss in photoactivity in our samples, especially at the highest sintering temperature.

Attempts to reduce the surface oxygen deficiency by preoxidizing the samples were made in two ways: (a) oxygen purging of the solution while the sample was kept polarized under potentiostatic conditions, or (b) by annealing the samples at 500 or 800°C in flowing oxygen gas. As seen in Fig. 4, oxygen purging for 5 min resulted in a significant increase in photoactivity which was most pronounced for the Mg-doped samples sintered at 1480°C. ESCA measurements of a Mg-doped iron oxide sample were taken before and after oxygen purging. The spectra (Fig. 2) show a substantial increase in oxygen content following the oxygen treatment. Before oxygen purging, the O(1*s*) peaks for both the Fe_2O_3 lattice (529.2 eV) and the peak for MgO and adsorbed oxygen (532.0 eV) are present. After the oxygen treatment only the higher binding energy peak is visible indicating the presence of a significant amount of adsorbed oxygen and hydroxyl species. This change in the surface composition of the iron oxide samples greatly improves their photoactivity (see Figs. 3 and 4).

Grain boundaries and weakly or partially bonded surface atoms are known to provide surface states with energies between the valence and conduction band edges (*19*). We believe that as the oxygen and hydroxyl ions strongly chemisorb on the surface a sufficient amount of free energy is released to shift these surface or grain boundary states outside of the bandgap region. This displacement would result in increased free electron lifetimes and reduced recombination rates of photoelectrons produced, which could explain the increased photoactivity of the oxygen treated samples. It is interesting to note that after oxygen purging all three samples show similar photoactivities. This indicates that an equilibrated carrier concentration state is reached during oxygen purging which is different from the carrier concentration states obtained upon rapid quenching from different sintering temperatures.

Previously, we reported that the photocurrents obtained with illumination of the Mg-doped iron oxide disks used as cathodes in a *p/n* diode assembly are directly proportional to the amount of hydrogen produced (*6*). These experiments included oxygen purging of the solution to regenerate the iron oxide electrodes. Even with this oxygen treatment the hydrogen production and observed photocurrents were well correlated. The effect of the oxygen treatment in the three electrode photoelectrochemical experiments, however, is quite large (Figs. 3 and 4) and one cannot exclude the possibility of O_2 reduction contributing to the currents measured.

Annealing the samples at 500 or 800°C in flowing oxygen gas had no beneficial effect on photoactivity. As discussed earlier the reason is a marked increase in resistivity after this oxidation pretreatment caused by the oxidation of grain boundaries of the ferric oxide matrix.

The effect of different Mg-doping levels is illustrated in Fig. 5 for 0.01 *N* NaOH and in Fig. 6 for 0.1 *M* Na_2SO_4. In both solutions the higher doping levels (10–20 at.%) result in higher *p*-type photocurrents at more cathodic applied potentials, presumably as a result of lower resistivities at higher Mg dopings. The onset potential for *p*-type photocurrent production, on the other hand, is higher (more anodic), the lower the Mg-doping levels are (see Table II). This behavior is qualitatively explained by the variation of the width of the space charge region which decreases with increasing doping level. Near the onset potential the space charge region approaches near flat-band conditions. From this it follows that the space charge width rather than the sample resistivity seems to be of critical importance for preventing electron hole recombination near flat-band conditions. Higher polarizations result in stronger band bending and the sample resistivity rather than the space charge width seems to have the strongest influence on the photocurrents obtained.

While *n*-type iron oxide shows a monotonic increase in photoactivity with the pH of the NaOH solutions (*6*) the pH dependence of the photoactivity for *p*-type iron oxide is different. As illustrated in Fig. 7 the photocurrent for the same Mg-doped sample was highest in 0.01 *N* NaOH and significantly lower in less basic and in more basic NaOH solutions. Assuming simple H^+/OH^- equilibria at the iron oxide surface the pH of the solution should have no effect on band bending or other thermodynamic criteria required for efficient photoelectrolysis of water. This has been verified on a number of oxide photoanodes (*20*). The strong pH dependence on the photoactivity of *n*-type $SrTiO_3$ has been suggested to be due to the involvement of hydroxide ions in a rate-limiting step, such as the formation

TABLE 2

ONSET POTENTIALS (mV) OF *p*-TYPE Mg-DOPED IRON OXIDES VS RHE (±50 mV)

	Solution:	0.1 *N* NaOH			0.1 *M* Na_2SO_4
Mg/(Mg + Fe) (at.%)	Sintering temperature:	1350°C	1425°C	1480°C	1350°C
1		900			900
5		950	900	700	850
10		990			850
20		825			650

of surface hydroxyl groups, which act as hole acceptors and thereby decrease the probability of electron-hole recombination (*21*). Similar arguments on *p*-type photocathodes would imply that a larger surface concentration of hydrogen ions, acting as electronacceptors, could also decrease the probability of electron-hole recombination. The reason why a peak in photoactivity is obtained around 0.01 *N* NaOH is, however, not clear and is the subject of further investigations.

Acknowledgments

This work was supported by the Director, Office of Energy Research, Office of Basic Energy Sciences, Chemical Sciences Division of the U.S. Department of Energy under Contract DE-AC03-76SF00098. We are greatly indebted to D. Neiman and J. Turner for valuable assistance.

References

1. W. H. Strehlow and E. L. Cook, *J. Phys. Chem. Ref. Data* **2,** 163 (1973).
2. D. S. Ginley and M. A. Butler, *J. Appl. Phys.* **48,** 2019 (1977).
3. M. A. Butler and D. S. Ginley, *J. Appl. Phys.* **48,** 3070 (1977).
4. I. T. Liou, C. Y. Yang, and S. N. Levine, *J. Electrochem. Soc.* **129,** 342 (1982).
5. H. Yoneyama, H. Sakamoto, and H. Tamura, *Electrochim. Acta* **20,** 341 (1975).
6. C. Leygraf, M. Hendewerk, and G. A. Somorjai, *J. Catal.* **78,** 341 (1982).
7. R. Shinar and J. H. Kennedy, *Sol. Energy Mater.* **1,** 237 (1979).
8. A. M. Redon, J. Vigneron, R. Heindl, C. Sella, C. Martin, and J. P. Dalbera, *Sol. Cells* **3,** 179 (1981).
9. R. F. Gardner, F. Sweett, and D. W. Tanner, *J. Phys. Chem. Solids* **24,** 1183 (1963).
10. J. Haber, J. Stoch, and L. Ungier, *J. Electron Spectrosc. Relat. Phenom.* **9,** 459 (1976).
11. K. L. Hardee and A. J. Bard, *Electrochem. Soc.* **123,** 1024 (1976).
12. R. K. Quinn, R. D. Nasby, and R. J. Baughman, *Mater. Res. Bull.* **11,** 1011 (1976).
13. L. S. R. Yeh and N. Hackerman, *J. Electrochem. Soc.* **124,** 833 (1977).
14. O. N. Salmon, *J. Phys. Chem.* **65,** 550 (1961).
15. F. J. Morin, *J. Phys. Rev.* **83,** 1005 (1951); **93,** 1195 (1954).
16. R. Shinar and J. H. Kennedy, *Sol. Energy Mater.* **67,** 323 (1982).
17. R. F. Gardner, F. Sweett, and D. W. Tanner, *J. Phys. Chem. Solids* **24,** 1175 (1963).
18. P. Merchant, R. Collins, R. Kershaw, K. Dwight, and A. Wold, *J. Solid State Chem.* **27,** 307 (1979).
19. A. Heller, *ACS Symp. Ser. A* (J. Nozik, Ed.) **146,** 57 (1981).
20. J. M. Bolts and M. S. Wrighton, *J. Phys. Chem.* **80,** 2641 (1976).
21. F. T. Wagner and G. A. Somorjai, *J. Amer. Chem. Soc.* **102,** 5474 (1980).